# Non-Invasive Differentiation of Benign Renal Tumors from Clear Cell Renal Cell Carcinomas Using Clinically Translatable Hyperpolarized $^{13}$C Pyruvate Magnetic Resonance

**Renuka Sriram[1], Mark Van Criekinge[1], Justin DeLos Santos[1], Kayvan R. Keshari[2], David M. Wilson[1], Donna Peehl[3], John Kurhanewicz[1], and Zhen J. Wang[1]**

[1]Radiology and Biomedical Imaging, University of California San Francisco, San Francisco, California; [2]Radiology and Molecular Pharmacology Program, Memorial Sloan Kettering Cancer Center, New York, New York; and [3]Department of Urology, Stanford University, Stanford, California

**Corresponding Author:**
Zhen Jane Wang, MD
Department of Radiology and Biomedical Imaging,
University of California, San Francisco, San Francisco, CA 94143
E-mail: jane.wang@ucsf.edu

**Key Words:** hyperpolarized $^{13}$C magnetic resonance, dynamic nuclear polarization, aerobic glycolysis, lactate efflux, renal cell carcinoma, patient-derived tissue slice cultures

**Abbreviations:** 2-dimensional (2D), 3-dimensional (3D), hyperpolarized (HP), lactate dehydrogenase (LDH), monocarboxylate 1 (MCT1), monocarboxylate 4 (MCT4), magnetic resonance (MR), magnetic resonance spectroscopy (MRS), dynamic nuclear polarization (DNP), renal cell carcinoma (RCC), clear cell renal cell carcinoma (ccRCC), nucleoside triose phosphate (NTP), monocarboxylate transporter (MCT), lactate dehydrogenase (LDH), hematoxylin and eosin (H&E), messenger ribonucleic acid (mRNA), complimentary deoxyribonucleic acid (cDNA),quantitative reverse transcription polymerase chain reaction (qRTPCR), nicotinamide adenine dinucleotide (NADH), phosphocholine (PC), inorganic phosphate (Pi), glycerol phosphocholine (GPC), choline kinase-alpha (CHKA), epidermal growth factor receptor (EGFR), signal-to-noise ratio (SNR)

ABSTRACT

Incidental detection of localized renal tumors at imaging is increasing. Conventional imaging cannot reliably differentiate the 20% of these tumors that are benign from malignant renal cell carcinomas (RCCs), leading to unnecessary surgical resection and resulting morbidity. Here, we investigated hyperpolarized $^{13}$C pyruvate metabolism in live patient-derived renal tumor tissue slices using a novel magnetic resonance-compatible bioreactor platform. We show, for the first time, that clear cell RCCs (ccRCCs), which constitute 70%–80% of all RCCs, exhibit increased lactate production and rapid lactate efflux when compared with benign renal tumors. This difference is because of increased lactate dehydrogenase A and monocarboxylate transporter 4 expression in ccRCCs. Thus, RCCs can be differentiated from benign renal tumors by assessing this distinctive metabolic phenotype using clinically translatable hyperpolarized $^{13}$C pyruvate magnetic resonance.

## INTRODUCTION

The widespread use of cross-sectional imaging has significantly increased incidental detection of renal tumors (1), many of which are localized, clinical stage I tumors. These tumors show a wide spectrum of benign and malignant histopathology, as well as aggressiveness, posing significant challenges for clinical management. Approximately 20% of clinical stage I renal tumors are benign tumors, such as oncocytomas or minimal fat angiomyolipomas (2-5). These benign tumors cannot be reliably differentiated from renal cell carcinoma (RCC) preoperatively by using conventional imaging (6). Percutaneous tumor biopsy is limited by low negative predictive value for small renal masses and overlapping histological features between some benign renal tumors and RCCs (7). Consequently, localized renal tumors are frequently treated with surgical resection, resulting in more than 10,000 unnecessary operations of benign tumors each year in the USA alone (8), with inherent risks of surgery, loss of renal function, and cost. Therefore, new noninvasive imaging methods are needed to distinguish benign renal tumors from RCCs to guide management.

RCCs are strongly linked to abnormal metabolism (9-11). In particular, clear cell RCCs (ccRCCs), which constitute 70%–80% of all RCCs, have a characteristic reprogramming of glucose and energy metabolism that promotes glycolysis and lactate production (12, 13). High expression of monocarboxylate transporters (MCT) 1 and 4, which are essential for maintaining high levels of glycolysis and lactate transport, is associated with more aggressive RCCs (14-16). These studies provide the rationale for metabolic imaging as a means to differentiate benign renal tumors from RCCs.

Hyperpolarized (HP) $^{13}$C magnetic resonance (MR) is a powerful molecular imaging technique that rapidly and noninvasively evaluates dynamic metabolic and physiological processes that were previously inaccessible by imaging (17). HP $^{13}$C pyru-


ISSN 2379-1381 http://dx.doi.org/10.18383/j.tom.2016.00106

vate is the most widely studied probe to date (18, 19), reflecting its central role in cellular metabolism. In particular, pyruvate is reduced to lactate in a reaction catalyzed by the enzyme lactate dehydrogenase (LDH). Several previous studies have shown that in vivo HP $^{13}$C pyruvate to lactate flux correlates with tumor stage in preclinical cancer models (20, 21).

In this study, we compared the HP $^{13}$C lactate levels after injecting HP $^{13}$C pyruvate in live patient-derived renal tissue slices maintained in an MR-compatible bioreactor. The bioreactor provides a novel platform for assessing tissue metabolism in a controlled and physiological setting (22, 23). ccRCCs showed high lactate production and, importantly, increased lactate export when compared with benign renal tumors. Thus, such metabolic phenotype can be explored to noninvasively differentiate ccRCCs from benign renal tumors using clinically translatable HP $^{13}$C pyruvate MR.

## MATERIAL AND METHODS

### Patient-Derived Renal Tissue Slices

Fresh tissues were obtained from patients undergoing nephrectomy for renal tumors between September 2012 and August 2014 under an institutional review board-approved protocol. Tissue cores (8-mm diameter) of both tumors and adjacent uninvolved normal renal parenchyma were obtained from the nephrectomy specimen (24). Tissues were precision-cut into 300- to 350-$\mu$m-thick slices using a Krumdieck Slicer (Alabama Research and Development, Mundford, Alabama), and then cultured in an incubator at 37°C and 5% $CO_2$ for 12–18 hours in a specialized medium in an angled, rotating plate (30°) as previously described (25). Subsequently, 4–6 tissue slices were loaded into a 5-mm MR-compatible bioreactor as previously described (22, 23) for the HP experiments described below. Patient-derived renal slices were obtained from 10 ccRCCs (Fuhrman grade 1: n = 1; Fuhrman grade 2: n = 8; and Fuhrman grade 3: n = 1), 3 benign renal tumors (oncocytomas: n = 2 and angiomyolipomas: n = 1), and 12 normal renal parenchyma tissues. These fresh tissue slices were studied in a 3-dimensional (3D) tissue bioreactor.

### MR-Compatible 3D Tissue Culture Bioreactor Experiments

The tissue slices were maintained at physiological conditions in the bioreactor in circulating media at 37°C with 95% air/5% $CO_2$ via a gas exchanger. All bioreactor experiments were conducted using a 500 MHz Varian Inova (Agilent Technologies, Palo Alto, California) with a 5-mm, triple-tune, direct-detect broadband probe. For the HP $^{13}$C pyruvate studies, 7.5 $\mu$L of 14.2 M [1-$^{13}$C]pyruvate, mixed with 15 mM of the trytl radical (GE Health, Menlo Park, California) and 2.5 mM of gadolinium chelate, was polarized on a Hypersense polarizer (Oxford Instruments, Oxford, UK), followed by dissolution in 5 mL of 50 mM phosphate buffer. Next, 750 $\mu$L of the resulting 16 mM of HP $^{13}$C pyruvate solution was injected over 90 seconds into the bioreactor containing the tissue slices. HP $^{13}$C MR data were dynamically acquired with a 30° flip angle, pulse repetition time of 3 seconds, and for a duration of 300 seconds. $^{31}$P spectra were acquired before and after each HP $^{13}$C study to assess tissue viability using a repetition time of 2 seconds, 2048 averages, and a 90° flip angle. The $\beta$-nucleoside triosephosphate ($\beta$NTP) peak was quantified using the electronic reference to access in vivo concentrations (ERETIC) method as described previously (26).

### Immunohistochemical Staining and Pathological Staging

At the end of the MR experiments, some of the renal tissue slices were rapidly frozen in a cryo-embedding medium (optimal cutting temperature compound) for subsequent histological and immunohistochemical analyses. A clinical pathologist determined the renal tumor histology and stage (Fuhrman nuclear grading if RCCs) on the basis of hematoxylin and eosin staining. In addition, the slices were stained for MCT4 expression.

### Tissue Slice mRNA Expression and Enzyme Activity Assay

Remaining tissue slices at the end of the bioreactor experiment were immediately frozen and used to measure the enzymatic activity and mRNA expression as described previously (22, 26). The mRNA expression of lactate dehydrogenase A (LDHA), MCT1, and MCT4 was quantified by quantitative reverse transcription polymerase chain reaction. In brief, total RNA was extracted from the tissue slices using an RNAeasy Kit (Qiagen, Germantown, Maryland). Reverse transcription was performed using an iScript cDNA Synthesis Kit (BioRad Laboratories, Hercules, California), and, subsequently, the complementary DNA generated was used for polymerase chain reaction in triplicate with TaqMan Chemistry on ABI 7900HT (Applied Biosystems, Foster City, California). Gene primers were obtained from Applied Biosystems, and gene expression was calculated relative to the housekeeping gene $\beta$-actin.

LDH activity of tissue slices was spectrophotometrically measured by quantifying the linear decrease in nicotinamide adenine dinucleotide absorbance at varying pyruvate concentrations at 339 nm using a microplate reader (Tecan Group Ltd., Mannedorf, Switzerland) (22, 26). The maximum velocity ($V_{max}$) and the Michaelis–Menten constant ($K_m$) were estimated using the Lineweaver–Burke plot, and were normalized to the protein content.

### Lactate Efflux Measurement of Renal Tissue Slices

Tissue slices immediately adjacent to those used in the bioreactor experiments were incubated in 2-dimensional (2D) culture in media containing 25 mM [3-$^{13}$C]pyruvate. The rate of lactate efflux from the tissue slices was evaluated by sampling the medium every 60–120 minutes over 8 hours. The lactate in the medium was measured by $^{1}$H MR spectroscopy in an 800 MHz Bruker DRX Spectrometer (Billerica, Massachusetts) equipped with a cryo-cooled 5-mm triple-axis heteronuclear probe. The J-coupled $^{13}$C satellite resonance was quantified using ACD/Labs software (Toronto, Canada) as described below.

### Data Analysis

The MR data were processed and analyzed using ACD/Labs software. The $^{13}$C data were processed with minimal line broadening, and the dynamic data were summed and expressed as a ratio of the HP $^{13}$C lactate peak area to $^{13}$C pyruvate area to normalize any differences in polarization across experiments. All data are represented as mean ± standard deviation. Two-

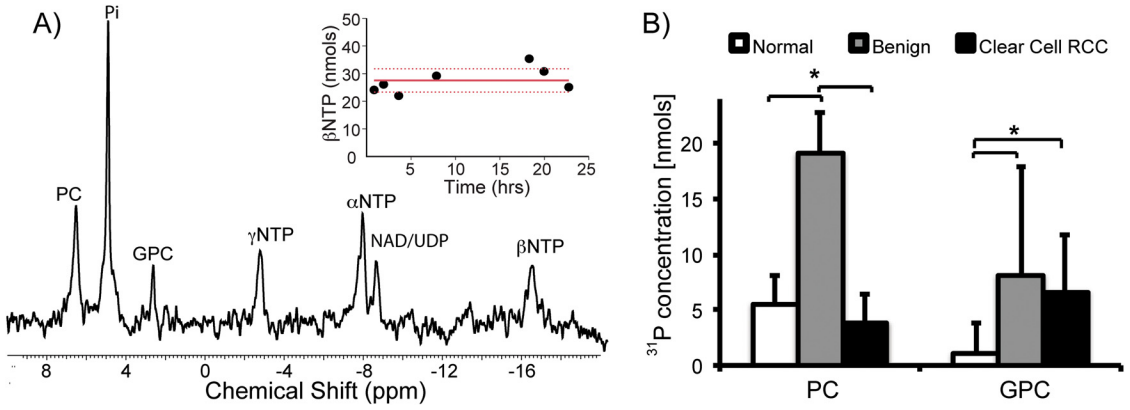


**Figure 1.** Bioenergetics of renal tissue slices. $^{31}$P spectrum of tissue slices (~80 mg) from a grade 2 ccRCC tissue (A). The inset shows the maintenance of tissue viability with unchanged βNTP concentration of tissue slices continuously perfused in the bioreactor for over 24 hours. Bar graph of the varying levels of phospholipids in renal tissue slices (n = 10 for normal renal parenchymal tissue, n = 10 for ccRCCs, and n = 3 for benign renal tumors) (B). PC concentration in the benign renal tumors is significantly higher than that in both the normal renal parenchyma ($P$ = .019) and ccRCC ($P$ = .008) tissues. In contrast, GPC was significantly higher in both benign renal tumors and ccRCCs compared with that in normal renal parenchyma tissue ($P$ = .027 and .003, respectively). White bars indicate normal renal parenchymal tissue, gray bars indicate benign renal tumors, and black bars indicate ccRCCs, with standard deviation error bars.

tailed Student $t$ test was used to assess the difference between groups.

## RESULTS

### Bioenergetics and Viability of Renal Tissue Slices in the MR-Compatible 3D Tissue Culture Bioreactor

In a prior study, we showed that the MR-compatible 3D bioreactor maintains tissue viability and provides reproducible HP $^{13}$C MR data (22). In this study, we used an MR-compatible 3D bioreactor for evaluating the metabolic activity of 60–90 mg of living tissue, and obtained excellent $B_0$ field homogeneity (average water line width at half maximum was 12.2 ± 0.68 Hz). $^{31}$P MR spectroscopy was used to monitor changes in renal tissue slice bioenergetics during the bioreactor studies. Figure 1A shows a representative $^{31}$P spectrum of ccRCC tissue slices. Nuclear magnetic resonance signals for the NTPs (γNTP, αNTP, and βNTP), nicotinamide adenine dinucleotide/uridine diphosphates, phosphocholine (PC), inorganic phosphate, and glycerol phosphocholine (GPC) were readily visible. The βNTP content was unchanged after the HP $^{13}$C pyruvate injection, indicating maintenance of tissue bioenergetics during the course of HP experiments.

Figure 1B shows the varying levels of phospholipids in the renal tissue slices. Interestingly, the PC level in the benign renal tumors was significantly higher than that in either the normal renal parenchyma ($P$ = .019) or ccRCC ($P$ = .008) tissues. This finding is similar to that from a prior $^{1}$H high-resolution study of renal tissue extracts (27). Although PC is used as a biomarker of proliferation and aggressiveness in other types of cancer (28), it has limited value in stratifying renal tumor aggressiveness. PC is converted from choline by the enzyme choline kinase-alpha in the phosphatidylcholine synthesis (Kennedy) pathway. A prior study reported that a functional interaction among choline kinase-alpha, epidermal growth factor receptor, and c-Src is required for cell proliferation (29). Such functional interactions may explain the lack of a direct correlation between the PC level and renal tumor aggressiveness in our study. In contrast, GPC was significantly higher in both benign renal tumors and ccRCCs when compared with normal renal parenchyma tissue ($P$ = .027 and .003, respectively). Although GPC is an osmolyte in the renal medulla, it is also involved in cell membrane recycling (30). The biological basis of elevated GPC levels in the renal tumor tissues requires further investigation.

### HP $^{13}$C Pyruvate Metabolism of Renal Tissue Slices in the 3D MR-Compatible Bioreactor

Figure 2A illustrates the scheme of $^{13}$C-labeled carbon flux used to detect [1-$^{13}$C]pyruvate metabolism during the HP MR experiment. After the injection of HP [1-$^{13}$C]pyruvate into the bioreactor, the $^{13}$C lactate level in the renal tissue slices was assessed in real time. The $^{13}$C lactate spectrum had excellent signal-to-noise ratio of 15 ± 2 (Figure 2B). The benign renal tumors and ccRCCs showed 2.7- and 1.7-fold higher HP $^{13}$C lactate levels (Figure 2C), consistent with increased aerobic glycolysis, when compared with normal renal parenchymal tissues ($P$ = .023 and .017, respectively). However, the observed $^{13}$C lactate level was 59% lower in ccRCCs than in benign renal tumors. Prior studies of human RCC cells in a similar continuous perfusion system showed that rapidly exported $^{13}$C lactate quickly flows out of the MR-sensitive volume without contributing to the measured HP $^{13}$C lactate signal (26). Therefore, we hypothesized that the apparent lower $^{13}$C lactate level in ccRCC than in benign renal tumors may be because of the rapid lactate efflux in ccRCCs, and we tested this hypothesis in the lactate efflux measurements described below.

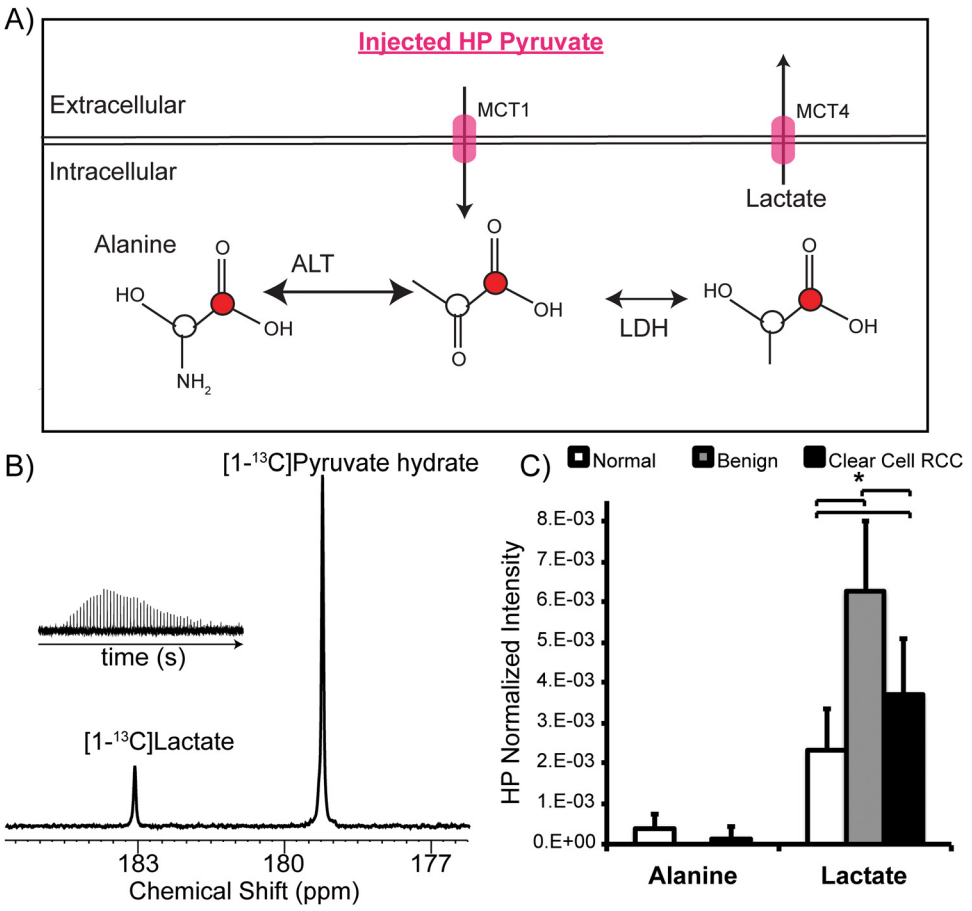


**Figure 2.** HP [1-$^{13}$C]pyruvate metabolism of renal tissue slices. Schematic illustrating the metabolism of HP [1-$^{13}$C]pyruvate to [1-$^{13}$C] lactate and [1-$^{13}$C] alanine, catalyzed by LDH and alanine aminotransaminase (ALT), respectively (A). $^{13}$C pyruvate is transported intracellularly via MCT1, and $^{13}$C lactate is exported out of the cells via MCT4. Representative hyperpolarized $^{13}$C spectrum of grade 2 ccRCC tissue slices (B). Inset shows the lactate kinetics over 5 minutes. Bar graphs of normalized HP [1-$^{13}$C] lactate and [1-$^{13}$C] alanine to the injected pyruvate in the tissue slices (C). Benign renal tumors and ccRCCs show 2.7- and 1.7-fold higher HP $^{13}$C lactate levels, consistent with increased aerobic glycolysis compared with normal renal parenchymal tissues. The observed $^{13}$C lactate level is 59% lower in ccRCCs than in benign renal tumors. White bars indicate normal renal tissue, gray bars indicate benign renal tumors, and black bars indicate ccRCC, with standard deviation error bars.

HP $^{13}$C alanine was consistently detected in the normal renal tissues with a signal-to-noise ratio of at least 3. Alanine was not detectable in the benign renal tumor tissues. Low alanine levels were occasionally observed (in ~30% of the cases) in the ccRCC tissues, consistent with our previous study showing lower alanine levels in immortalized human RCC cells than in normal renal tubular cells (26).

### Tissue Analysis Confirming ccRCCs Show Higher Lactate Production and Efflux than Benign Renal Tumors:

To test the hypothesis that ccRCCs show higher lactate production and efflux than benign renal tumors, we assayed the mRNA expression and enzymatic activity of LDH and mRNA expression of MCT1 and MCT4 in the tissue slices. The *LDHA* gene encodes the M subunits of LDH, which catalyzes the conversion between pyruvate and lactate. MCT1 mediates pyruvate transport into cells, and MCT4 mediates the efflux of lactate out of the cells (31, 32). Mean LDHA mRNA expression was significantly higher in ccRCCs (171 ± 106) than in either normal renal tissues (41 ± 25) or benign tumors (50 ± 36) ($P$ = .001 and .016, respectively; Figure 3A). Correspondingly, the LDH activity was significantly higher in ccRCC than in normal renal tissues ($P$ = .020) and benign tumors ($P$ = .030), by 2.4- and 1.7-fold, respectively (Figure 3A). Similarly, mRNA expression of MCT1 (Figure 3B) was significantly higher in ccRCCs than in normal renal tissues (3-fold higher, $P$ = .006) and benign tumors (8-fold higher, $P$ = .002). The higher expression of LDHA and MCT1 in ccRCCs when compared with that in benign renal tumors is consistent with an increase in glycolysis and lactate production in ccRCCs.

MCT4 expression was significantly higher in ccRCCs as seen by the progressively increased MCT4 staining from normal renal tissues when compared with ccRCCs (Figure 4A). Correspondingly the mRNA expression was significantly higher in ccRCCs than in normal renal tissues (4-fold higher, $P$ = .021) and benign tumors (11-fold higher, $P$ = .045; Figure 4B). Corresponding immunohistochemical staining also showed progressively. These data suggest that ccRCCs show a high rate of lactate efflux. To further verify that the higher MCT4 expression in ccRCCs caused increased lactate efflux, we quantified the lactate efflux rate in the tissue slices in a 2D culture by labeling with [3-$^{13}$C]pyruvate (Figure 4C). The incubation medium was sampled intermittently for up to 8 hours, and the [3-$^{13}$C]lactate level was measured using high-resolution nuclear magnetic resonance spectroscopy. The normal renal tissues and benign tumors

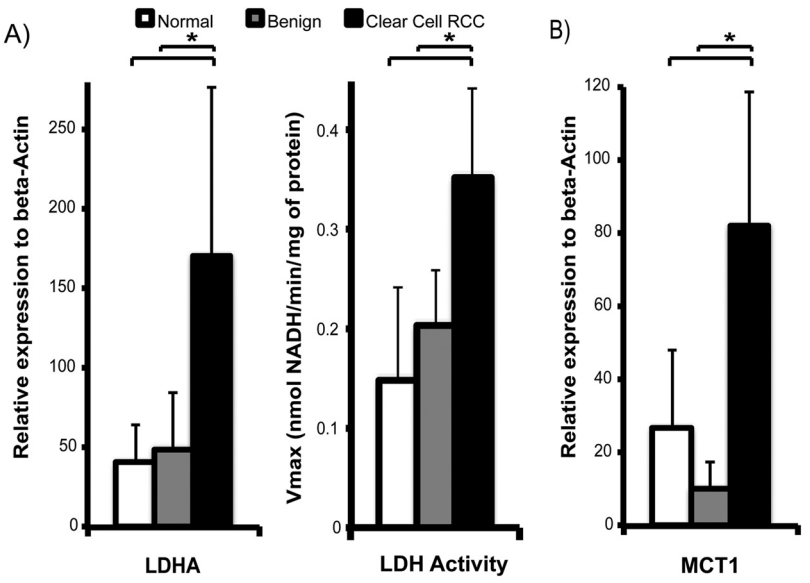


**Figure 3.** LDHA expression and LDH activity and MCT1 expression in renal tissue slices. Mean LDHA mRNA expression is higher in ccRCCs than in either normal renal tissues or benign tumors ($P$ = .001 and .016, respectively), and the LDH activity was also correspondingly higher in ccRCC than in either normal renal tissues ($P$ = .020) or benign tumors ($P$ = .030) (A). MCT1 expression is significantly higher in ccRCCs than in both normal renal tissues ($P$ = .006) and benign tumors ($P$ = .002) (B). The sample size of the tissues used for mRNA analyses is as follows: n = 11 for normal renal tissue, n = 3 for benign renal tumors, and n = 7 for ccRCCs. White bars indicate normal renal tissue, gray bars indicate benign renal tumors, and black bars indicate ccRCC, with standard deviation error bars.

had similar lactate efflux rates of 1.83 ± 1.98 nmol/min and 2.32 ± 0.89 nmol/min, respectively, whereas ccRCCs had a significantly higher efflux rate of 5.04 ± 1.82 nmol/min ($P$ = .013 and .002, respectively). Taken together, these observations support the hypothesis that ccRCCs show the highest lactate production and efflux compared with benign renal tumors and normal renal tissues. The rapid lactate efflux out of the cells is a dominant factor resulting in the observed apparent lower HP $^{13}$C lactate levels in ccRCCs than in benign renal tumors.

## DISCUSSION AND CONCLUSION

An unmet need in the management of patients with localized renal tumors is the lack of imaging biomarkers that can reliably discriminate benign tumors from RCCs. In this study, we investigated pyruvate metabolism in live patient-derived renal tumor tissues using HP [1-$^{13}$C]pyruvate, an HP $^{13}$C MR probe that has been used in patient studies (33). We showed that high lactate production and rapid lactate efflux are characteristic features of ccRCC, which constitutes the majority of RCCs, and that this metabolic feature may help differentiate malignant from benign renal tumors.

Increasing evidence has shown that RCCs are strongly linked to abnormal metabolism (9, 10, 34). Specifically, increased glycolysis with lactate production is a dominant metabolic feature of many RCCs. Lactate is exported out of the cells, predominantly mediated by MCT4, a proton-coupled lactate transporter. Rapid lactate export plays a key role in maintaining high levels of lactate production, acidifying the tumor interstitium, and promoting invasion and metastasis, all key features of cancer (35, 36). A recent study showed that MCT4 protein expression in ccRCCs is associated with poorer relapse-free survival and correlates with the Fuhrman nuclear grade (15). In our present study, we showed that live patient-derived ccRCC tissues show more rapid lactate efflux, because of high MCT4 expression, when compared with benign renal tumors. Such differential expression and the resultant lactate efflux rate may be explored noninvasively using HP $^{13}$C MR. In this pre-clinical study which utilized an ex vivo system, the higher lactate export in RCCs compared to benign tumors was inferred from a combination of HP $^{13}$C MR and steady-state labeling experiments. However, it is possible to discriminate the local environment of HP metabolites using diffusion-weighted HP $^{13}$C MR in vivo (37). Our findings provide rationale for such in vivo studies, and there is ongoing research for using in vivo diffusion-weighted HP $^{13}$C MR to directly assess the relative amount of intracellular versus extracellular lactate. In addition, in vivo HP imaging will also permit the assessment of total lactate as a marker of lactate production in renal tumors. During the time frame of the HP studies, the lactate exported out of the renal tumor cells is likely to remain within the tumor interstitium, and the combined intra- and extracellular lactate can then be measured. Lactate production and lactate efflux rate can provide complementary biomarkers of renal tumor aggressiveness.

The development of novel imaging markers of RCC presence and aggressiveness has been impeded by the lack of robust models that recapitulate human disease. Available preclinical models are predominantly based on immortalized aggressive RCC cells either grown in culture or implanted in animals. We previously studied pyruvate metabolism in immortalized RCC cells (26), but we were unable to investigate the metabolism of benign renal tumors, as there are currently no preclinical models of benign human renal tumors. Immortalized RCC cells also have unusually high proliferation indices when compared with patient-derived renal tumor tissues, which may be reflected in the observed metabolism. Furthermore, immortalized cell models do not capture the complex tumor cell–matrix interactions that occur in human

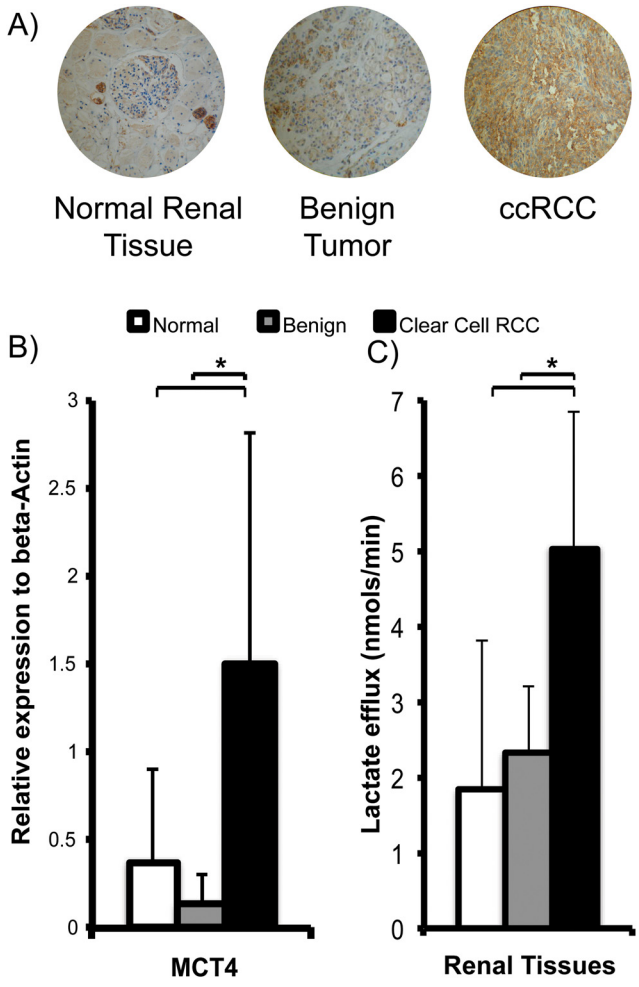


**Figure 4.** Renal tissue MCT4 expression and lactate efflux. Representative images of MCT4 immunohistochemical staining show increased MCT4 staining (brown staining) in ccRCCs compared with benign renal tumors and normal renal parenchymal tissues (A). ccRCCs show the highest MCT4 mRNA expression compared with normal renal parenchymal tissues ($P = .021$) and benign renal tumors ($P = .045$) (B). ccRCCs show the highest rate of lactate efflux compared with normal renal parenchymal tissues ($P = .013$) and benign renal tumors ($P = .002$) (C). The sample size is as follows: $n = 11$ for normal renal tissue, $n = 3$ for benign renal tumors, and $n = 7$ for ccRCCs. White bars indicate normal renal tissue, gray bars indicate benign renal tumors, and black bars indicate ccRCC, with standard deviation error bars.

renal tumors, and which are likely important for tumor metabolism. To overcome these difficulties, we used, in this study, a patient-derived renal tumor slice model for assessing the metabolism in intact living human tissues. The novel MR-compatible microengineered bioreactor permits evaluation of living tissue metabolism in a physiological environment, and this has been previously validated by our group in prostate cancer studies (22). The combination of primary human renal tumor tissue slices and MR-compatible bioreactor provides a unique and realistic model for HP $^{13}$C biomarker discovery in renal tumors before patient studies.

The main limitation of our study is the small number of benign renal tumors. A high percentage of tumor tissues used in this study were from radical nephrectomy of large renal tumors (average size of 6.6cm). The proportion of benign tumors was low in this patient cohort since benign tumors tend to be smaller in size, and more likely to be treated with partial nephrectomy. Nonetheless, we have shown a significant difference in both the hyperpolarized $^{13}$C data and the tissue correlative findings between benign tumors and RCCs. The results of the study provide motivation for future clinical studies of HP $^{13}$C pyruvate MR in patients with renal tumors. Another limitation of our study is that we have only included clear cell RCCs, and not other subtypes of RCCs. This in part reflects the fact that clear cell RCCs comprises majority of RCCs (70-80%), and we did not obtain sufficient number of other subtype of RCCs to include in our analysis. Along the same line, the majority of the clear cell RCC tissues obtained were grade 1 or 2; there was an insufficient number of higher grade (grade 3 or 4) clear cell RCCs to perform separate analysis based on grade. Future studies are warranted to assess any potential grade dependent findings. Future studies can assess any potential grade-dependent findings. Development of imaging markers that can reliably differentiate low- from high-grade RCCs is of great clinical interest given the increasing recognition that low-grade indolent RCCs may be conservatively treated via active surveillance rather than surgical resection (38). Third, the renal tumor tissue slices used in the 2D culture experiments were not the same as those used in the 3D bioreactor experiments. Although renal tumors do have intratumoral heterogeneity, the tumor tissue slices were from the same core and were immediately adjacent to each other. Therefore, any potential heterogeneity is not likely to affect the overall results.

Notwithstanding these limitations, we showed that high lactate production and rapid lactate efflux are dominant features of ccRCCs. These features can be explored to noninvasively differentiate cancers from benign renal tumors using HP $^{13}$C pyruvate MR, particularly when combined with diffusion weighting. These initial findings provide a strong basis for developing HP $^{13}$C MR for clinical evaluation of renal tumors. The safety and feasibility of HP $^{13}$C pyruvate has been shown in a phase I clinical trial in patients with prostate cancer (33), which opens doors for potential clinical translation of this technology to other diseases. In addition, there is ongoing research for developing multichannel $^{13}$C MR coil to provide optimal signal reception in abdominal organs for clinical studies. These

technical advances will translate this emerging molecular imaging tool for the assessment of renal tumors, a disease of increasing frequency, with the ultimate goal of guiding treatment selection.

## ACKNOWLEDGMENTS

We thank Rosalie Nolley, Romelyn Delos Santos, Laura Tabatabai, Ailin Hansen, Dave Korenchen, Sukumar Subramaniam, Bertram Koelsch, and Jessie Lee for assistance in performing experiments.

This work was supported by National Institutes of Health (R01 EB013427, R01 EB017449, R01 CA183071, P41 EB013598, R21 EB005363, R00 EB014328, P30 CA008748, R01 CA166655, and R01 DK097357) and the Department of Defense (USAMRMC CA110032).

Quantitative reverse transcription polymerase chain reaction analysis was conducted at the Genome Analysis Core Facility, Helen Diller Family Comprehensive Cancer Center, University of California, San Francisco.

Conflict of Interest: None Reported

Disclosure: No disclosures to report.

## REFERENCES

1. Sun M, Thuret R, Abdollah F, Lughezzani G, Schmitges J, Tian Z, Shariat SF, Montorsi F, Patard JJ, Perrotte P, Karakiewicz PI. Age-adjusted incidence, mortality, and survival rates of stage-specific renal cell carcinoma in North America: a trend analysis. Eur Urol. 2010 ed. 2011 Jan; 59(1):135–141.
2. Frank I, Blute ML, Cheville JC, Lohse CM, Weaver AL, Zincke H. Solid renal tumors: an analysis of pathological features related to tumor size. J Urol. 2003 Dec; 170( 6 Pt 1): 2217–2220.
3. DeRoche T, Walker E, Magi-Galluzzi C, Zhou M. Pathologic characteristics of solitary small renal masses: can they be predicted by preoperative clinical parameters? Am J Clin Pathol. 2008 Oct; 130(4):560–564.
4. Snyder ME, Bach A, Kattan MW, Raj GV, Reuter VE, Russo P. Incidence of benign lesions for clinically localized renal masses smaller than 7 cm in radiological diameter: influence of sex. J Urol. 2006 Dec; 176( 6 Pt 1): 2391–2395; discussion 2395-2396.
5. Murphy AM, Buck AM, Benson MC, McKiernan JM. Increasing detection rate of benign renal tumors: evaluation of factors predicting for benign tumor histologic features during past two decades. Urology. 2009 Jun; 73(6):1293–1297.
6. Woo S, Cho JY. Imaging findings of common benign renal tumors in the era of small renal masses: differential diagnosis from small renal cell carcinoma: current status and future perspectives. Korean J Radiol. 2015 Jan-Feb; 16(1):99–113.
7. Ljungberg B, Hanbury DC, Kuczyk MA, Merseburger AS, Mulders PFA, Patard J-J, Sinescu IC. European Association of Urology Guideline Group for renal cell carcinoma. Renal cell carcinoma guideline. Eur Urol. 2007; 51(6):1502–1510.
8. Asnis-Alibozek AG, Fine MJ, Russo P, McLaughlin T, Farrelly EM, LaFrance N, Lowrance W. Cost of care for malignant and benign renal masses. Am J Manag Care. 2013 Aug; 19(8):617–624.
9. Pinthus JH, Whelan KF, Gallino D, Lu J. P, Rothschild N. Metabolic features of clear-cell renal cell carcinoma: mechanisms and clinical implications. Can Urol Assoc J 2011 Aug; 5(4):274–282.
10. Zaravinos A, Pieri M, Mourmouras N, Anastasiadou N, Zouvani I, Delakas D, Deltas C. Altered metabolic pathways in clear cell renal cell carcinoma: A meta-analysis and validation study focused on the deregulated genes and their associated networks. Oncoscience. 2014 Jan; 1(2):117–131.
11. Hakimi AA, Reznik E, Lee C. H, Creighton CJ, Brannon AR, Luna A, Aksoy BA, Liu EM, Shen R, Lee W, Chen Y, Stirdivant SM, Russo P, Chen Y. B, Tickoo SK, Reuter VE, Cheng EH, Sander C, Hsieh JJ. An integrated metabolic atlas of clear cell renal cell carcinoma. Cancer Cell. 2016 Jan; 29(1):104–116.
12. Unwin RD, Craven RA, Harnden P, Hanrahan S, Totty N, Knowles M, Eardley I, Selby PJ, Banks RE. Proteomic changes in renal cancer and co-ordinate demonstration of both the glycolytic and mitochondrial aspects of the Warburg effect. Proteomics. 2003 Aug; 3(8):1620–1632.
13. Singer S, Souza K, Thilly WG. Pyruvate utilization, phosphocholine and adenosine triphosphate (ATP) are markers of human breast tumor progression: a 31P- and 13C-nuclear magnetic resonance (NMR) spectroscopy study. Cancer Res. 1995 Nov; 55(22):5140–5145.
14. Fisel P, Kruck S, Winter S, Bedke J, Hennenlotter J, Nies AT, Scharpf M, Fend F, Stenzl A, Schwab M, Schaeffeler E. DNA methylation of the SLC16A3 promoter regulates expression of the human lactate transporter MCT4 in renal cancer with consequences for clinical outcome. Clin Cancer Res. 2013 Sep; 19(18):5170–5181.
15. Fisel P, Stühler V, Bedke J, Winter S, Rausch S, Hennenlotter J, Nies AT, Stenzl A, Scharpf M, Fend F, Kruck S, Schwab M, Schaeffeler E. MCT4 surpasses the prognostic relevance of the ancillary protein CD147 in clear cell renal cell carcinoma. Oncotarget. 2015 Oct; 6(31):30615–30627.
16. Gerlinger M, Santos CR, Spencer-Dene B, Martinez P, Endesfelder D, Burrell RA, Vetter M, Jiang M, Saunders RE, Kelly G, Dykema K, Rioux-Leclercq N, Stamp G, Patard J. J, Larkin J, Howell M, Swanton C. Genome-wide RNA interference analysis of renal carcinoma survival regulators identifies MCT4 as a Warburg effect metabolic target. J Pathol. 2012 Apr; 227(2):146–156.
17. Keshari KR, Wilson DM. Chemistry and biochemistry of 13C hyperpolarized magnetic resonance using dynamic nuclear polarization. Chem Soc Rev. 2014 Mar; 43(5):1627–1659.
18. Sriram R, Kurhanewicz J, Vigneron DB. Hyperpolarized carbon-13 MRI and MRS studies. eMagRes. 2014 Dec; 3(4):311–324. http://dx.doi.org/10.1002/9780470034590.emrstm1253
19. Chaumeil MM, Najac C, Ronen SM. Studies of metabolism using (13)C MRS of hyperpolarized probes. Methods Enzymol. 2015; 561: 1–71.
20. Albers MJ, Bok R, Chen AP, Cunningham CH, Zierhut ML, Zhang VY, Kohler SJ, Tropp J, Hurd RE, Yen Y. F, Nelson SJ, Vigneron DB, Kurhanewicz J. Hyperpolarized 13C lactate, pyruvate, and alanine: noninvasive biomarkers for prostate cancer detection and grading. Cancer Res. 2008 Oct; 68(20):8607–8615.
21. Kurhanewicz J, Vigneron DB, Brindle K, Chekmenev EY, Comment A, Cunningham CH, DeBerardinis RJ, Green GG, Leach MO, Rajan SS, Rizi RR, Ross BD, Warren WS, Malloy CR. Analysis of cancer metabolism by imaging hyperpolarized nuclei: prospects for translation to clinical research. Neoplasia. 2011 Feb; 13(2):81–97.
22. Keshari KR, Sriram R, Van Criekinge M, Wilson DM, Wang ZJ, Vigneron DB, Peehl DM, Kurhanewicz J. Metabolic reprogramming and validation of hyperpolarized 13C lactate as a prostate cancer biomarker using a human prostate tissue slice culture bioreactor. Prostate. 2013 Aug; 73(11):1171–1181.
23. Keshari KR, Wilson DM, Van Criekinge M, Sriram R, Koelsch BL, Wang ZJ, VanBrocklin HF, Peehl DM, O'Brien T, Sampath D, Carano RAD, Kurhanewicz J. Metabolic response of prostate cancer to nicotinamide phosphoribosyltransferase inhibition in a hyperpolarized MR/PET compatible bioreactor. Prostate. 2015 Oct; 75(14):1601–1609.
24. Thong AE, Zhao H, Ingels A, Valta MP, Nolley R, Santos J, Young SR, Peehl DM. Tissue slice grafts of human renal cell carcinoma: an authentic preclinical model with high engraftment rate and metastatic potential. Urol Oncol. 2014 Jan; 32(1): 43.e23-30.
25. Maund SL, Nolley R, Peehl DM. Optimization and comprehensive characterization of a faithful tissue culture model of the benign and malignant human prostate. Lab Invest. 2014 Feb; 94(2):208–221.
26. Keshari KR, Sriram R, Koelsch BL, Van Criekinge M, Wilson DM, Kurhanewicz J, Wang ZJ. Hyperpolarized 13C-pyruvate magnetic resonance reveals rapid lactate export in metastatic renal cell carcinomas. Cancer Res. 2013 Jan; 73(2):529–538.
27. Tugnoli V, Poerio A, Tosi MR. Phosphatidylcholine and cholesteryl esters identify the infiltrating behaviour of a clear cell renal carcinoma: 1H, 13C and 31P MRS evidence. Oncol Rep. 2004 Aug; 12(2):353–356.
28. Podo F. Tumour phospholipid metabolism. NMR Biomed. 1999 Nov; 12(7):413–439.
29. Miyake T, Parsons SJ. Functional interactions between Choline kinase $\alpha$, epidermal growth factor receptor and c-Src in breast cancer cell proliferation. Oncogene. 2011 Aug; 31(11):1431–1441.
30. Glunde K, Bhujwalla ZM, Ronen SM. Choline metabolism in malignant transformation. Nat Rev Cancer. 2011 Dec; 11(12):835–848.
31. Dimmer KS, Friedrich B, Lang F, Deitmer JW, Bröer S. The low-affinity monocarboxylate transporter MCT4 is adapted to the export of lactate in highly glycolytic cells. Biochem J. 2000 Aug; 350 Pt 1: 219–27.
32. Harris T, Eliyahu G, Frydman L, Degani H. Kinetics of hyperpolarized 13C1-pyruvate transport and metabolism in living human breast cancer cells. Proc Natl Acad Sci USA. 2009 Oct; 106(43):18131–18136.
33. Nelson SJ, Kurhanewicz J, Vigneron DB, Larson PEZ, Harzstark AL, Ferrone M, Van Criekinge M, Chang JW, Bok R, Park I, Reed G, Carvajal L, Small EJ, Munster P, Weinberg VK, Ardenkjaer-Larsen JH, Chen AP, Hurd RE, Odegardstuen L. I., Robb FJ, Tropp J, Murray JA. Metabolic Imaging of Patients with Prostate Cancer Using Hyperpolarized [1-13C]Pyruvate. Sci Transl Med. 2013 Aug; 5(198): 198ra108.

34. Yang OCY, Maxwell PH, Pollard PJ. Renal cell carcinoma: translational aspects of metabolism and therapeutic consequences. Kidney Int. 2013 Oct; 84(4):667–681.
35. Parks SK, Chiche J, Pouysségur J. Disrupting proton dynamics and energy metabolism for cancer therapy. Nat Rev Cancer. 2013 Aug; 13(9):611–623.
36. Gatenby RA, Gillies RJ. A microenvironmental model of carcinogenesis. Nat Rev Cancer. 2008 Jan; 8(1):56–61.
37. Koelsch BL, Reed GD, Keshari KR, Chaumeil MM, Bok R, Ronen SM, Vigneron DB, Kurhanewicz J, Larson PEZ. Rapid in vivo apparent diffusion coefficient mapping of hyperpolarized (13) C metabolites. Magn Reson Med. 2015 Sep; 74(3):622–633.
38. Van Poppel H, Joniau S. Is surveillance an option for the treatment of small renal masses? Eur Urol. 2007 Nov; 52(5):1323–1330.